Polymer 51 (2010) 6071–6083

Contents lists available at ScienceDirect

Polymer

journal homepage: www.elsevier.com/locate/polymer

Molecular dynamics simulations of deformation mechanisms of amorphous polyethylene

D. Hossain, M.A. Tschopp*, D.K. Ward, J.L. Bouvard, P. Wang, M.F. Horstemeyer

Center for Advanced Vehicular Systems (CAVS), Mississippi State University, Mississippi State, MS 39762, USA

ARTICLE INFO

Article history:
Received 4 June 2010
Received in revised form
1 October 2010
Accepted 6 October 2010
Available online 15 October 2010

Keywords:
Molecular dynamics simulation
Polyethylene
Deformation mechanisms

ABSTRACT

Molecular dynamics simulations were used to study deformation mechanisms during uniaxial tensile deformation of an amorphous polyethylene polymer. The stress-strain behavior comprised elastic, yield, strain softening and strain hardening regions that were qualitatively in agreement with previous simulations and experimental results. The chain lengths, number of chains, strain rate and temperature dependence of the stress-strain behavior was investigated. The energy contributions from the united atom potential were calculated as a function of strain to help elucidate the inherent deformation mechanisms within the elastic, yield, and strain hardening regions. The results of examining the partitioning of energy show that the elastic and yield regions were mainly dominated by interchain nonbonded interactions whereas strain hardening regions were mainly dominated by intra-chain dihedral motion of polyethylene. Additional results show how internal mechanisms associated with bond length, bond angle, dihedral distributions, change of free volume and chain entanglements evolve with increasing deformation.

1. Introduction

Polymers play an important role in materials science as a candidate for future new industrial materials, primarily because their properties can be tuned very easily. The flexibility of tuning polymer's properties comes from a number of available degrees of freedom: choice of monomers, branching, tacticity, copolymers, blends and composites [1]. The particular polymer studied here is polyethylene (PE), a common material for commercial goods.

Polymeric systems are highly complex in nature. Computational modeling of polymers has assisted in understanding their complex behavior. However, no single modeling technique, to this point, has adequately captured all of the large length and time scales associated with polymers. The large length and time scale issues associated with polymers suggest implementing a multiscale modeling scheme [2]. Coarse grain techniques [3–10], such as united atom [4,5], have been widely used to simulate polymer systems at various length and time scales.

The molecular origin of plastic deformation within amorphous polymers is an important issue that is still not well understood [2]. Initially, it was assumed that plastic deformation in glassy polymers occurs due to shear stress, which could induce structural change by altering the energy barriers of structural rearrangement within the solid [11]. Roberson later postulated that the shear stress would alter the flexing of dihedral angles creating a local pocket of material with liquid-like molecular mobility [12]. In line with this notion, Argon [13] developed a model that treats shear strain as the accumulation of rotations of kink pairs along the polymer chains. Some insight into the role of shear strain during deformation can be gleaned from atomistic studies of plastic deformation in bulk metallic glasses. For instance, Deng et al. [14] used MD simulations of atomic glasses to predict that plastic deformation occurs as a result of local rearrangements which produce shear transformation. The shear transformations essentially act as nucleation sites for additional transformations, the percolation of which eventually produces localized flow structures. Using molecular statics (MS), Maeda and Takeuchi [15] and Srolovitz et al. [16] studied the deformation behavior of three-dimensional metallic glasses. In these studies, they observed that plastic deformation is a result of highly localized heterogeneous atomic rearrangements which generate local stresses that considerably exceed the applied stress. Although the studies of atomic/metallic glasses provide interesting insights into the deformation behavior of relatively simple systems, the complex bonding along the polymer backbone makes investigations of glassy polymers considerably more difficult.

Atomistic simulations have provided insight into the deformation behavior of polymers. Theodorou and Suter [17,18] first attempted to model the mechanical response of glassy polymers by probing the

* Corresponding author.
E-mail address: mtschopp@cavs.msstate.edu (M.A. Tschopp).

0032-3861/$ – see front matter © 2010 Elsevier Ltd. All rights reserved.
doi:10.1016/j.polymer.2010.10.009

elastic properties of glassy polypropylene using MS techniques. Mott et al. [19] and Hutnick et al. [20] subsequently used this method to study the plastic deformation of polypropylene and polycarbonate, respectively. Mott et al. found that plastic deformation is a result of abrupt shear transformations which involve the cooperative motion of many degrees of freedom. These cooperative motions are a consequence of the highly constrained nature of the amorphous chain structure. In agreement with these findings, Hutnick et al. found that cooperative motions accommodate deformation in glassy polycarbonate, independent of the chemical specificity of them.

Similar atomistic studies investigated glassy polyethylene as well. Brown and Clarke [21] and Mckechnie and Clarke [22] used MD simulations to investigate the effects of thermal motion on deformation in glassy polyethylene and attempted to correlate the obtained response with experimental results. Despite the fact that the deformation rates used were much higher than experimental rates, they were able to qualitatively correlate the rate and temperature dependence of uniaxial tensile deformation with that of experimental results. Mckechnie and Clarke's investigation showed the effect that initial chain configuration properties have on the resulting mechanical response. Their results show that strain hardening can be enhanced by increasing either the persistence length or the fraction of *trans* conformers in the initial chain configuration.

Although several groups have studied the static, dynamic, and mechanical properties of PE systems [21,23–31], research on large PE systems, particularly mechanical properties, is still in its infancy. Molecular dynamics (MD) and Monte Carlo (MC) simulations have proven to be essential tools for exploring the static, dynamic and mechanical properties of bulk amorphous polymers at the molecular levels. Brown and Clarke [21] performed detailed studies of uniaxial deformation at various strain rates of an amorphous polyethylene-like polymer system containing 1000 united atoms. The simulated elastic deformation, yield, and plastic flow at low temperature qualitatively capture the experimental deformation behavior. Capaldi et al. [29] found that compressive deformation of a glassy PE-like polymer increases the transition rate between different dihedral angle states and promotes propagation of dihedral angle flips along the chain. Li et al. [32] carried out atomistic Monte Carlo (MC) simulations of uniaxial tension of an amorphous linear polyethylene (PE)-like glassy polymer. They investigated the temperature and strain rate dependencies on the stress-strain curve and found qualitative agreement with experimental results. Their investigation on conformation showed that during deformation the chains adopt more extended conformations, and the fraction of dihedrals in the *trans* state increases. The energy and stress portioning with increasing strain show that in the elastic region mechanical work is primarily stored as non-bonded internal energy in the material, whereas from the yield region onward the intra-chain contributions start to play a role. Ospina et al. [33,34] used MC simulation results of the initial stage of deformation of linear polyethylene (PE) using 2D lattice model. They observed a stress-strain behavior comparable to that observed in experiments, but neither strain softening nor strain hardening were reported [33–35].

The objective of this research is to study the relevant deformation mechanisms responsible for the different regimes (elasticity/yield/strain softening/strain hardening) observed during uniaxial tension deformation of glassy polyethylene using atomic-scale simulations with the united atom model. In this article, we investigate the stress-strain response for different chain lengths, number of chains and temperatures relative to the glass transition temperature. The stress-strain behavior of PE deformation and its dependence to the strain rate and temperature were studied and compared to previous theoretical and experimental results. To obtain insight into the role of different bonded and non-bonded interactions during PE deformation, we investigated in details the different contributions to the internal energy at different stages of deformation. We also evaluated internal mechanisms associated with bond length, bond angle, dihedral distributions, change of free volume and chain entanglements. Our main interest was correlating the stress-strain response to the deformation mechanisms responsible for the mechanical behavior.

2. Simulation methodology

2.1. Interatomic potential

The interatomic force field for polyethylene is based on a united atom model using the Dreiding potential [36]. There were several reasons why this potential was chosen. First, this study investigates uniaxial deformation of amorphous polyethylene systems with large numbers of monomers (20,000–200,000 united atoms) as a function of strain rates that vary over three orders of magnitude (10^8–10^{10} s^{-1}). Full-atom representations would require approximately three times the number of atoms (i.e., carbon plus two hydrogens) along with a more computationally-expensive force field and, quite possibly, a smaller timestep or different integration scheme due to adding hydrogen. Additionally, the 10^8 s^{-1} strain rate in these simulations requires millions of timesteps to reach strains of approximately 100%. Therefore, the use of the united atom model and Dreiding potential was influenced in part by the computational expense. Second, much of the prior literature regarding molecular dynamics simulations of polyethylene have used the Dreiding potential, e.g., Refs. [28,29]. In this sense, this work can build upon results previously obtained, while also providing guidance as to the influence of chain length, number of chains, temperature, and strain rates when moving to full-atom representations with optimized force fields. We leave deformation of full-atom polymer representations for future work.

The united atom model used here considers each methyl group (i.e., the CH_2 monomer) as a single atom with a force field that determines the interactions between united atoms. The Dreiding potential [36] is used to describe these interactions. The Dreiding potential has four contributing terms; bond stretching, changes in bond angle, changes in dihedral rotation, and van der Waals non-bonded interactions. The force field and its respective parameters for the PE system are given in the Table 1. The total force field energy can be expressed as

Table 1
Functional form of force field and potential parameters used for polyethylene MD calculations.

Interaction	Form	Parameters
Bond Length	$E_{\text{bond}}(r) = \frac{1}{2}K_b(r-r_0)^2$	$K_b = 350.0$ kcal/mol, $r_0 = 1.53$ Å
Bond Angle	$E_{\text{angle}}(\theta) = \frac{1}{2}K_\theta(\theta-\theta_0)^2$	$K_\theta = 60$ kcal/mol/rad^2, $\theta_0 = 1.911$ rad (109.5°)
Dihedral Angle	$E_{\text{dihedral}}(\phi) = \sum_{i=0}^{3} C_i(\cos\phi)^i$	$C_0 = 1.736$, $C_1 = -4.490$, $C_2 = 0.776$, $C_3 = 6.990$ (kcal/mol)
Non-bonded	$E_{\text{non-bonding}}(r) = 4\varepsilon\left[(\frac{\sigma}{r})^{12} - (\frac{\sigma}{r})^{6}\right],\ r \le r_c$	$\sigma = 4.01$ Å, $\varepsilon = 0.112$ kcal/mol

$$E_{total} = E_{bond}(r) + E_{angle}(\theta) + E_{dihedral}(\phi) + E_{non-bonding}(r) \quad (1)$$

In the present simulations, the interaction potential has two components which are summed over all possible atom combinations: bonded and non-bonded interaction terms. The bonded terms comprise bond stretching (r), bond angle bending (θ) and dihedral angle torsion (ϕ). The functional form of bonded energy is given as

$$E_{bond}(r) = \frac{1}{2}K_b(r - r_0)^2 \quad (2a)$$

$$E_{angle}(\theta) = \frac{1}{2}K_\theta(\theta - \theta_0)^2 \quad (2b)$$

$$E_{dihedral}(\phi) = \sum_{i=0}^{3} C_i(\cos\phi)^i \quad (2c)$$

where K_b and K_θ are the stiffness constants for the bond length and bond angle potentials, respectively, r_0 and θ_0 are the equilibrium bond length and bond angle, respectively, and the variable C_i contains the coefficients of dihedral multi-harmonic. For the parameters chosen in the present work, the global minimum of the dihedral potential is at 180°, which corresponds to the planar *trans* state (t). In addition, two local minima are located at 60° (*gauche*, g^+) and 300° (*gauche*, g^-), respectively.

The non-bonded or Van der Waals interactions are given by a Lennard-Jones potential, i.e.,

$$E_{non-bonding}(r) = 4\varepsilon\left[\left(\frac{\sigma}{r}\right)^{12} - \left(\frac{\sigma}{r}\right)^{6}\right], \; r \le r_c \quad (3)$$

where r is the distance between two atoms, σ is the distance at zero energy, and ε is the energy well depth. The cutoff distance r_c is taken as 10 Å. Table 1 gives the values for all of the constants used in the interatomic potential [37,38].

2.2. Deformation simulations

A parallel molecular dynamics code, LAMMPS [39], that incorporates domain decomposition was used to deform the polymer simulation cells. A Nosé-Hoover thermostat was used to regulate the system temperature [40–42]. Table 2 lists the different combinations of chain lengths and number of chains used in the simulation cell. The simulations were performed for three chain lengths (100, 1000, and 2000 monomers) with three different number of chains (20, 200 and 2000) for a total of 2×10^4–2×10^5 total united atoms. The mechanical responses for each simulation resulted from averages of three different initial configurations to account for entropic effects due to the high number of possible chain conformations. Three temperatures were examined: 100 K, 250 K, and 400 K. These temperatures were purposely chosen to select a low temperature (100 K), a temperature just below the glass transition temperature (250 K), and a temperature above the glass transition temperature (400 K). The simulation cell was orthogonal with a minimum length of 8 nm in each direction.

Table 2
Chain length, number of chains and total number of united atoms used for the different systems.

System	Chain Length (monomers)	Number of Chains	Total Number of United Atoms
1	100	200	20000
2	1000	20	20000
3	100	2000	200000
4	1000	200	200000

The initial chain structure was created using a method similar to those previously developed using Monte Carlo self-avoiding random walks [43]. The chain generation step used a face-centered cubic (FCC) lattice superimposed on the simulation cell with the nearest neighbor distance of 1.53 Å. Molecules were added to the lattice in a probabilistic stepwise manner, which based the probability of chain growth in certain directions on the bond angle and the density of unoccupied sites.

This initial structure was then inserted into the molecular dynamics code where an equilibration sequence was performed prior to deforming the amorphous polymer. The equilibration sequence relaxes any high energy configurations that are artificially created due to the FCC lattice used to generate the amorphous polymer structure. The relaxation involves four different steps. Initially, the simulation ran for 10^5 timesteps ($\Delta t = 1$ fs) using NVT dynamics at 500 K followed by relaxation for 5×10^5 timesteps ($\Delta t = 0.5$ fs) using NPT dynamics at 500 K. The next relaxation cooled the structure down to the desired temperature for 5×10^5 timesteps followed by further relaxation of 5×10^5 timesteps at the desired temperature.

The glass transition temperature was used to verify that such equilibration of the polymer structure was appropriate for deformation simulations. The glass transition temperature T_g, delimiting the glassy regime to the rubbery one, is an important characteristic of polymeric material. The glass transition temperature was determined from the change in slope of the specific volume vs. temperature curve [29,31,44–47]. First, the system was equilibrated at 500 K. Then, the system temperature was decreased from 500 K to 100 K over 5×10^5 fs (cooling rate of 0.8 K/ps). Fig. 1 shows a graph of the volume of the polymer as a function of temperature for a system consisting of 20 chains with 1000 monomers each. The intersection of the two linear trend lines fitted to the ends of the data gives an estimate of the glass transition temperature. Table 3 lists the calculated glass transition temperatures for systems with four different chain lengths and number of chains. The change in the glass transition temperature with the number of chains or chain lengths is small (<5K). The calculated values here are similar to those calculated by other groups using molecular dynamics

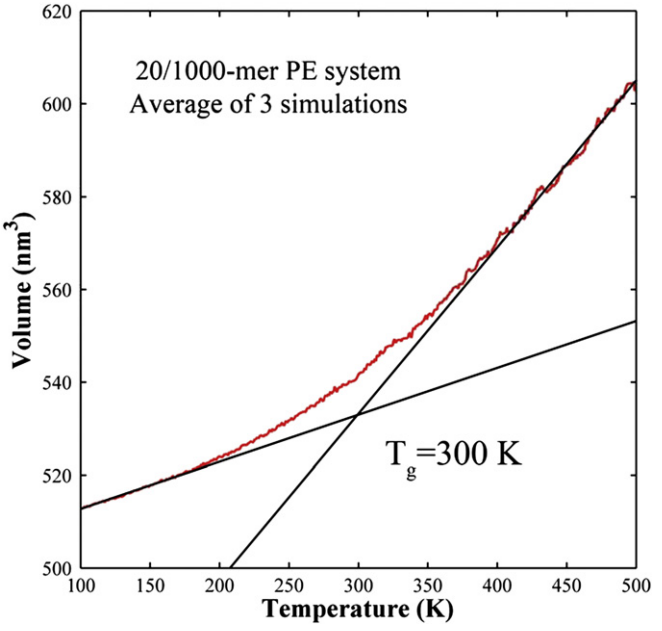

Fig. 1. Plot of volume evolution as a function of temperature, which was used for determining the glass transition temperature.

Table 3
Glass transition temperature of different polymeric systems.

Chain length/ number of chains	Total number of united atoms	Glass transition temperature (K)
100/200	20000	300.6
100/2000	200000	302.3
1000/20	20000	299.6
1000/200	200000	301.5

[29,31,44,46], which fall in the range of 250–300 K, close to the experimentally-measured value of 250 K [47]. As for the temperatures chosen for this study, Fig. 1 clearly shows that 100 K is in the glassy state and 250 K lies in the transition region between glassy and rubbery below the glass transition temperature. The interatomic potential does not allow bonds to break, so 400 K is best characterized as in the rubbery state.

The amorphous PE system was then deformed under a uniaxial tensile strain applied at a constant strain rate with a zero-pressure condition for the two lateral simulation cell faces. This deformation condition was implemented in LAMMPS by decoupling the boundary in the loading direction from the NPT equations of motion [48]. The stress components were calculated from the symmetric pressure tensor, which uses components from the kinetic energy tensor and the virial tensor. In addition to calculating the stress as a function of strain, the energy contributions associated with the bond length, bond angles, dihedral angle and non-bonding interactions were tracked as a function of strain. Periodic dumps of the atomic configuration were performed to compute additional microstructure metrics such as chain orientation or the percentage of *trans* dihedral conformations. Three different strain rates (10^8 s^{-1}, 10^9 s^{-1} and 10^{10} s^{-1}) were used with an initial configuration consisting of 20 polymeric chains, each having 1000 monomers, to investigate the effect of strain rate. To investigate the influence of chain length and chain number, polyethylene configurations were uniaxially deformed at a strain rate of 10^9 s^{-1} for different numbers of chains (100 and 2000) and chain lengths (20, 200, and 2000 monomers).

2.3. Microstructure characterization

After equilibrating the system, the microstructure of the polymer chain was characterized to ensure that the structure was appropriate for deformation simulations. Additionally, we utilized various internal microstructure metrics to characterize the initial polymer structure and to track its evolution as a function of strain in the deformation simulations.

The common microstructure metrics used to quantitatively assess the polymer chain geometry were the bond length, bond angle, and dihedral angles. Fig. 2 shows an example of the bond length, bond angle and dihedral angle distributions of a 20 chain, 1000 monomer PE system after equilibrating the system at 100 K. The average bond length for all equilibrated systems was 1.529 Å and the average bond angle was 109.27°. The average values were slightly lower than the equilibrium potential parameters r_0 and θ_0. The average bond lengths and bond angles were very similar for systems equilibrated at temperatures of 100 K and 250 K. However, the standard deviation of the bond length and bond angle distributions increases with increasing temperature, e.g., the average standard deviation for bond lengths at 100 K and 250 K were 0.0170 and 0.267 Å, respectively. The dihedral angle distribution has a broad distribution with both gauche and *trans* peaks. To calculate the fraction of *trans* conformations within the PE system, a threshold value of 120° was used to delineate the gauche peak (centered about 66°) from the trans peak (centered about 180°). The percent *trans* conformations in the initial structure was 73.8% and 68.3% for the 100 K and 250 K samples, respectively. The initial densities for the amorphous PE structures ranged from 0.87 to 0.91 g/cm^3, slightly lower than experimental values for low density polyethylene (0.91–0.94 g/cm^3), which contains a high degree of short and long chain branching. While these densities are slightly lower than experimental values, we deem this acceptable for the united atom method potential employed. In addition to tracking the evolution of the aforementioned microstructure features, we also tracked the evolution of other metrics related to the internal structure: polymer density, chain end-to-end distance, chain radius of gyration, and chain orientation.

3. Results

3.1. Stress-strain behavior

3.1.1. Different regimes

The isothermal stress-strain curve for PE of 1000 monomers chain length and total number of 20 chains deformed at 250 K for a strain rate of 10^{10} s^{-1} are shown in Fig. 3. The stress-strain curve has four distinct regimes: elastic, yield, softening and hardening. Initially the stress increases nearly linearly with increasing applied strain indicating an elastic regime. Upon reaching the yield point, the stress then shows a decrease to a local minimum suggesting material softening. Further deformation of PE causes an increase in

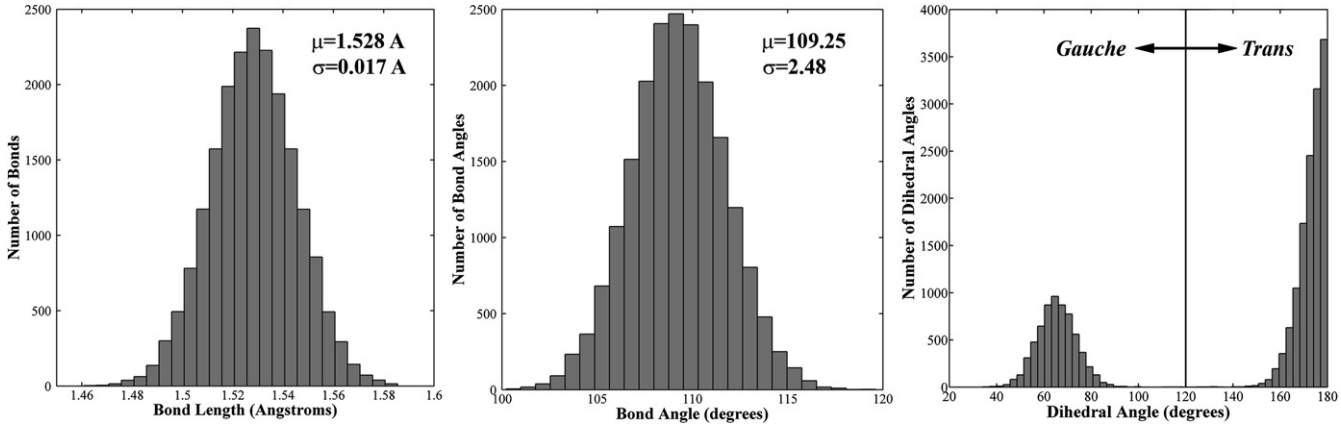

Fig. 2. The bond length, bond angle, and dihedral angle distributions for a 20 chain, 1000 monomer polyethylene system after equilibrating the system at 100 K.

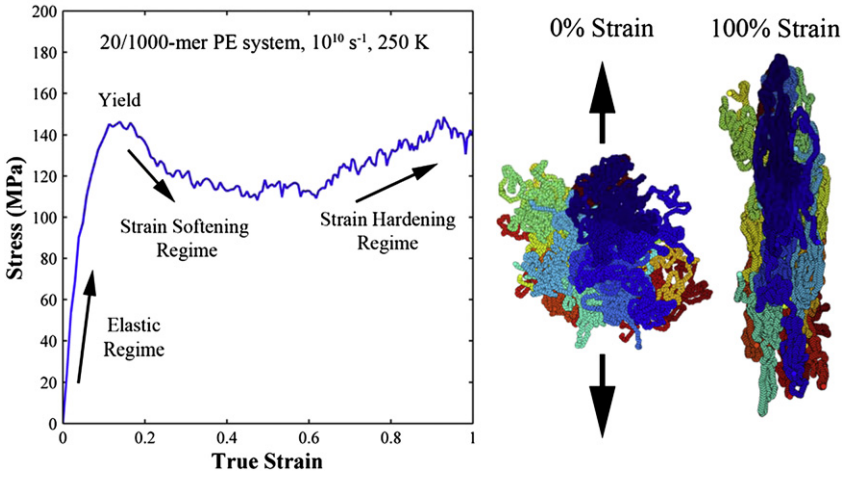

Fig. 3. Stress-strain response of a polyethylene (PE) glassy polymer deformed in uniaxial tension at strain rate of 10^{10}/s and temperature of 250 K. The accompanying images (right) show the polyethylene structure after equilibration and at 100% true strain (colors represent united atoms on separate chains).

stress and strain hardening. Similar behaviors were reported in molecular dynamics (MD) tension simulation [28,29,47] and in Monte Carlo (MC) compression simulation [32].

3.1.2. Chain length and number of chains dependence

The dependence on the deformation of PE on the chain lengths and the total number of chains were studied at a fixed deformation rate of 10^9 s^{-1} and temperature 250 K. Fig. 4 shows that the chain length has a more significant effect on the stress-strain curves than the number of chains. The curves follow the same behavior as discussed in the previous section except the strain softening is less pronounced in the smaller chain lengths. The higher chain lengths tend to have slightly stiffer elastic regimes, higher yield stresses and more predominant softening. This has previously been attributed to higher entanglement densities for longer chain length materials. With a higher number of chains, the curves are much smoother suggesting that the simulations move closer to a bulk behavior. Even though the larger simulations have a smoother response the smaller simulations still capture the necessary stress-strain behavior of the polymer.

3.1.3. Temperature dependence

The influence of temperature on the stress-strain behavior was also explored. Fig. 5 shows the stress-strain curves for a polymeric system represented by 20 chains with 1000 monomers each deformed using a strain rate of 10^9 s^{-1} at temperatures of 100 K, 250 K and 400 K. The change in the temperature shows a very clear effect on the polymer's stress-strain response. The material stiffness decreases with increasing temperature, as expected. At 100 K and 250 K, the stress-strain curve shows a typical elastic response followed by: yielding softening, and hardening. The yield point and softening regime is much more pronounced for 100 K. At 400 K (above the glass transition temperature), the stress-strain curve doesn't show any softening or subsequent strong material hardening.

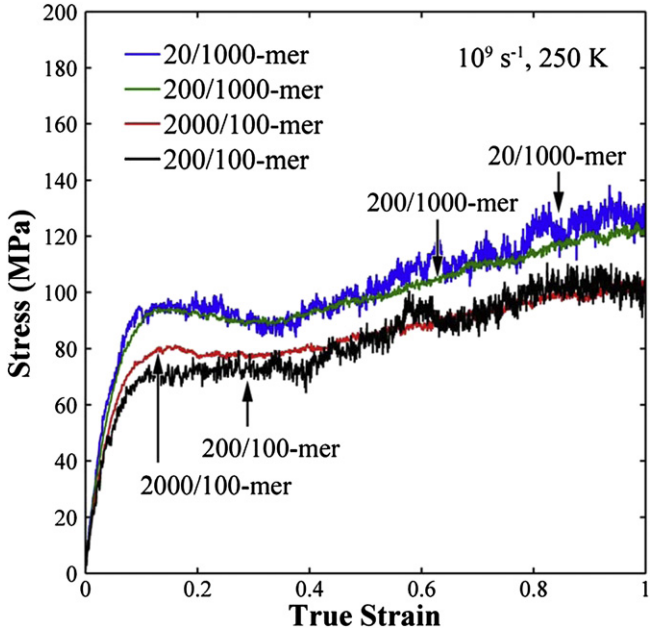

Fig. 4. Stress-strain response for different chain lengths and number of chains for a 10^9 s^{-1} strain rate at 250 K.

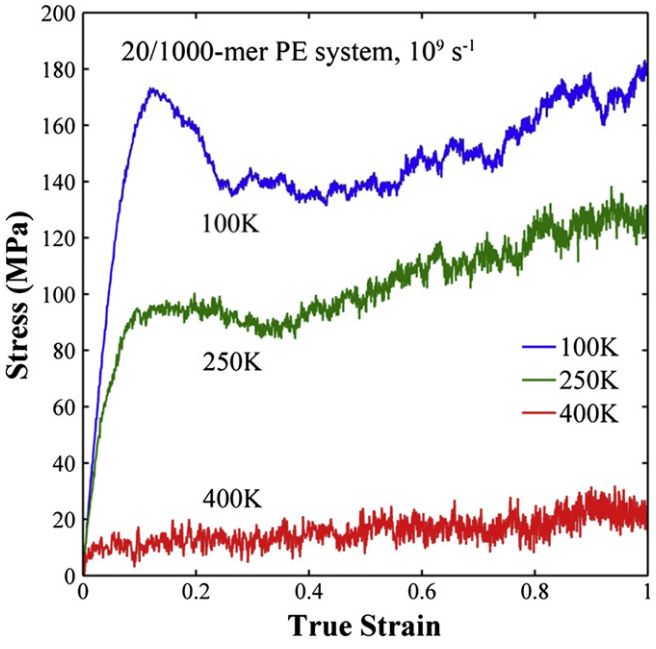

Fig. 5. Stress-strain response at a strain rate of 10^9 s^{-1} for different temperatures.

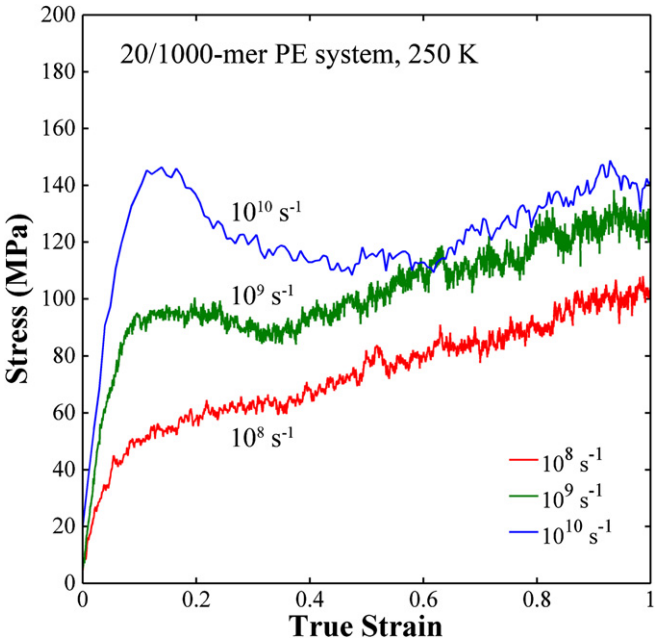

Fig. 6. Stress-strain response at 250 K for different strain rates.

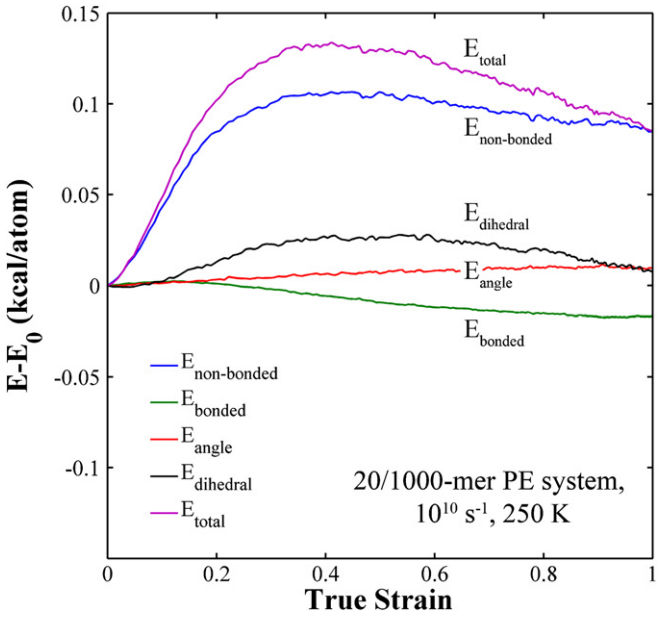

Fig. 7. Energy decomposition for a polyethylene (PE) system with 20 chains consisting of 1000 monomers each at 250 K for a strain rate of 10^{10} s^{-1}. The non-bonded energy changes most during the elastic regime, while the dihedral and bonded energy changes most during the strain softening/hardening regimes.

3.1.4. Strain rate dependence

Fig. 6 shows the stress-strain curves for a polymeric system represented by 20 chains with 1000 monomers each deformed at 250 K using strain rates of 10^8 s^{-1}, 10^9 s^{-1} and 10^{10} s^{-1}. The simulations at different strain rates exhibit different stress-strain curves. The stress-strain curve at a strain rate of 10^{10} s^{-1} follows the typical trend with an elastic regime, followed by yield, and then followed by a strain softening and strain hardening regime. The elastic modulus and peak yield stress increases with increasing strain rate. The trend of higher stresses for higher strain rates continues for the strain softening and strain hardening regimes as well. However, the mechanisms in these regimes may be similar since the strain hardening slope stays constant. The simulations show similar stress-strain responses with increasing strain rate as the simulations with decreasing temperature (in Section 3.1.3). The elastic moduli and peak yield stresses calculated from simulations at different strain rates and temperatures are given in Table 4. The elastic modulus and the yield stress increase with increasing strain rate and decreasing temperature. These trends are as expected and agree qualitatively with the experimental and computational theoretical results. The mechanisms responsible for the temperature and strain rate behavior will be discussed in Section 4.

3.2. Internal energy evolution

3.2.1. Different regimes

Fig. 7 illustrates the potential energy change of a PE system of 1000 monomers chain length and total number of 20 chains deformed at 250 K for a strain rate of 10^{10} s^{-1}, which corresponds to the stress-strain behavior observed in Fig. 3. In addition to the total energy E_{total}, the individual components of the energy are shown: the non-bonded energy E_{nb}, the bonding energy E_b, the bond angle energy E_a and the dihedral energy E_{dihed}. In the elastic region, the dihedral, angle and bond energies remain almost unchanged and a majority of the increase in total energy is correlated with an increase in the non-bonded energy, i.e., Van der Waal's forces between polymer chains. The non-bonded energy increases sharply in the elastic and strain softening regions, which can be associated with chain slippage mechanisms. After the elastic region, the non-bonded energy stays fairly constant while there are significant changes in the bond angle and dihedral energies. The energy associated with bond length steadily decreases as bond lengths move towards the equilibrium bond length. The dihedral angle energy increases in the strain softening regime and then steadily decreases in the strain hardening regime as *gauche* conformations rotate to the lower energy *trans* conformations. The total energy sharply increases in the elastic region due to non-bonded interactions and then slowly decreases over the strain softening and hardening regions as energy is dissipated via dihedral rotations and bond length changes to accommodate deformation.

Table 4
Elastic modulus and peak yield stress of PE at various temperatures and strain rates.

$\dot{\varepsilon}$ (s^{-1})	Temperature (K)	E (Mpa)	σ_Y (Mpa)
10^8	250	6.3×10^2	52
10^9	250	1.1×10^3	97
10^{10}	250	1.2×10^3	145
10^9	100	1.6×10^3	168
10^9	400	3.8×10^2	8

3.2.2. Chain length and number of chains dependence

Fig. 8 shows an example of an energy decomposition curve at 250 K for a strain rate of 10^9 s^{-1}, which is representative of the various chain number and chain length (100 and 1000 monomers) combinations. In general, the energy decomposition curves follow the same behavior for all chain lengths and chain numbers. However, there is less variability in the energy evolution curves for the PE systems with a higher amount of total united atoms, i.e., the example plot has 200,000 total united atoms and the least amount of noise. Also, notice a slightly different trend for the strain rate of 10^9 s^{-1} at 250 K than that displayed in Fig. 7 (10^{10} s^{-1} at 250 K). In Fig. 8, very little change in the energies associated with bond length and bond angle occur. However, the non-bonded energy still increases sharply during the elastic and strain softening regimes,

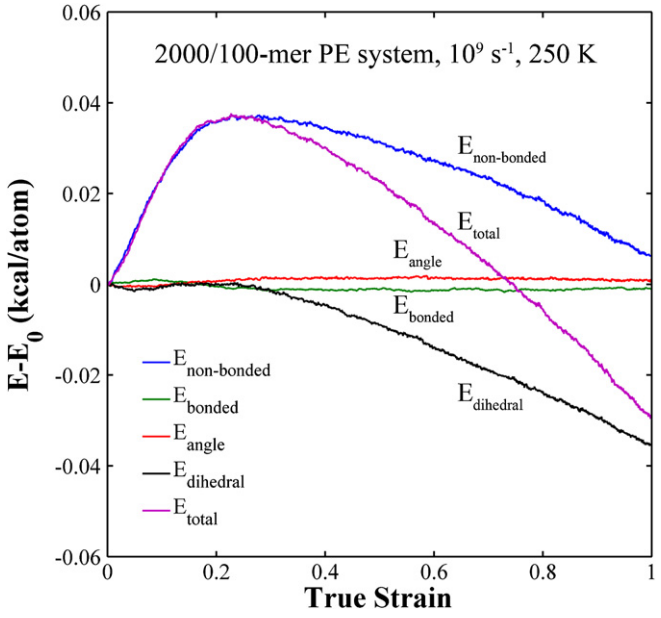

Fig. 8. Energy decomposition for a polyethylene system with 2000 chains consisting of 100 monomers each at 250 K for a strain rate of 10^9 s^{-1}. Similar trends were observed for other chain lengths and number of chains.

while dihedral energy plays a vital role in the strain hardening regime. Over all, though, the chain length and number of chains show very little effect on the energy decomposition.

3.2.3. Temperature dependence

Fig. 9(a–c) displays the energies associated with the non-bonded interactions, bond, angle and the dihedral rotation for a system of 1000 monomers chain length and total number of 20 chains deformed using a strain rate of 10^9 s^{-1} at temperatures of 100 K, 250 K, and 400 K. Again, the energy decomposition curves show that the energies associated with the bond length and bond angles do not change significantly. As a result, the majority of deformation in the polymer system is accommodated via dihedral rotations and non-bonded interactions. However, as depicted by Fig. 9(a) and (b), the energy evolution curves suggest that the molecular mechanisms at 100 K are slightly different than those at 250 K. At 100 K, the total and non-bonded interaction energy increased and then remains nearly constant, whereas the non-bonded interaction energy decreases in the strain softening and hardening regimes for 250 K. Additionally, the decrease in the dihedral energy is much greater for 250 K than at 100 K. The evolution of the internal energy during deformation at 400 K shown in Fig. 9(c) suggests a system whereby multiple coupled deformation modes are possible.

3.2.4. Strain rate dependence

Fig. 10(a–c) shows the variation in internal energy as a function of strain rate for the PE system with 20 chains of 1000 monomers each at 250 K. The strain rates applied here span two orders of magnitude and have a significant effect on the energy evolution. At the higher strain rate of 10^{10} s^{-1}, the behavior of the total energy and non-bonded interaction energy contributions are very different than that at the lowest strain rate of 10^8 s^{-1}. The behavior at strain rates of 10^{10} and 10^9 s^{-1} is as discussed previously. At a strain rate of 10^8 s^{-1}, there is very little change in the energies associated with bond length and bond angles with increasing strain. The non-bonded interaction energy increases slightly and then decreases with increasing strain. The dihedral angle (and total) energy

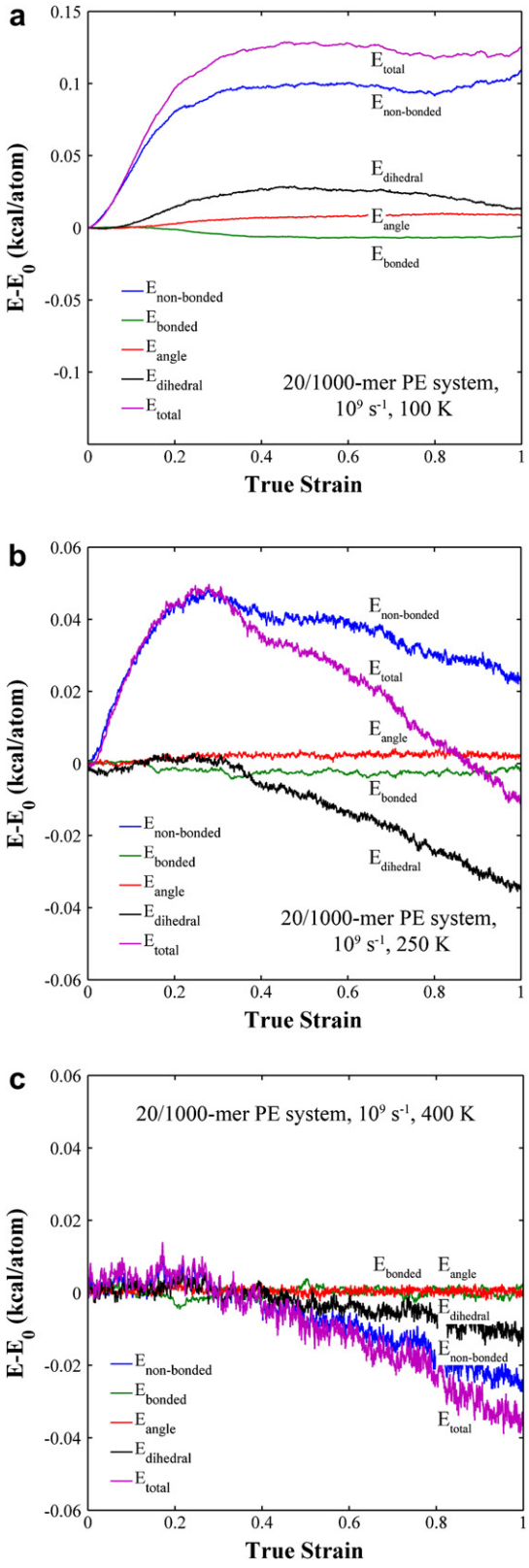

Fig. 9. (a–c): Energy decomposition for a polyethylene system with 200 chains consisting of 1000 monomers each at a strain rate of 10^9/s for different temperatures: 100 K, 250 K, and 400 K.

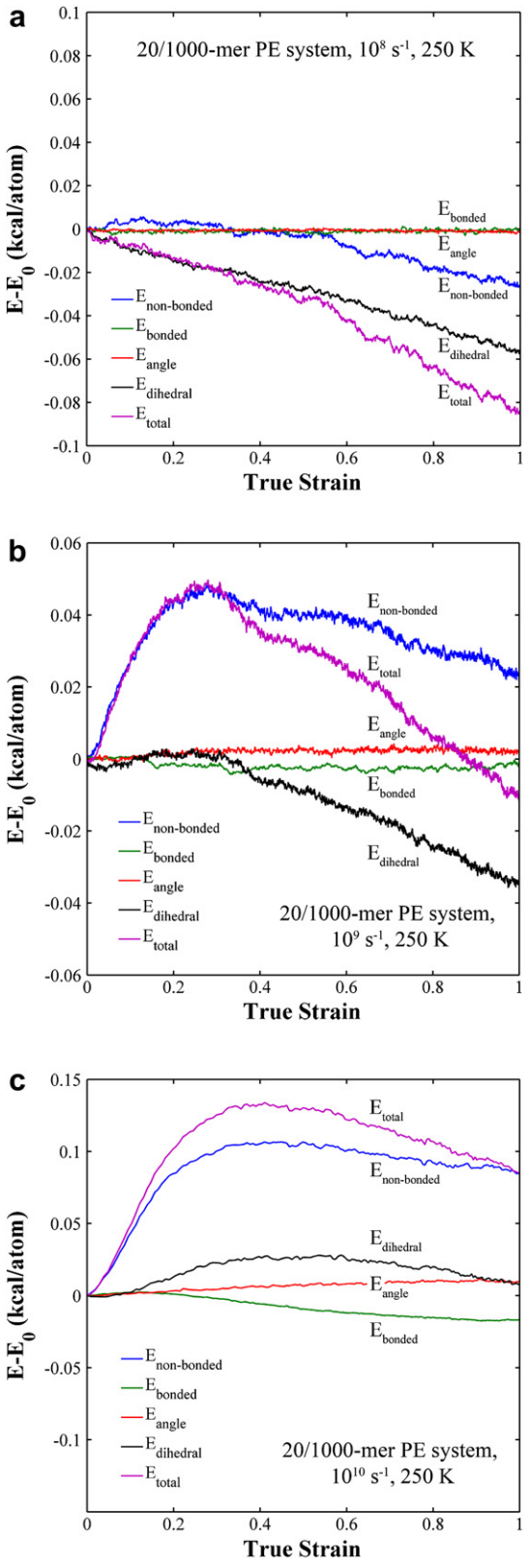

Fig. 10. (a–c): Energy decomposition for a polyethylene system with 20 chains consisting of 1000 monomers each deformed at 250 K for three different strain rates: 10^8 s^{-1}, 10^9 s^{-1}, and 10^{10} s^{-1}.

immediately decreases with increasing strain during the elastic region, unlike the behavior at the higher strain rates. Interestingly, because the dihedral energy decrease occurs during the elastic regime at a strain rate of 10^8 s^{-1}, the non-bonded interaction energy does not increase as sharply as higher strain rates, signifying a change in where the energy associated with deformation is accommodated at lower strain rates.

3.3. Evolution of internal structure variables

3.3.1. Free volume evolution

The evolution of the simulation cell volume (polymer density) as a function of strain should provide some information on the evolution of free volume within the amorphous PE structure. Therefore, as a first order approximation, we have considered the change in the simulation cell volume to be equivalent to the evolution of free volume during deformation. Fig. 11 shows the change in free volume as a function of strain for a system with 20 1000-mer chains for different strain rates at 250 K. The general trend is that the free volume increases with increasing strain in the elastic region, which is followed by a slight decrease to steady behavior in the latter strain hardening region. As the strain rate is increased, the free volume increase observed in the elastic regions also increases. At a strain rate of 10^8 s^{-1}, the free volume continuously decreased as the material is deformed. Fig. 12 shows the change in free volume as a function of strain for different chain lengths and number of total chains (100/200, 1000/20, 1000/200 and 100/2000 systems). Fig. 12 shows that the free volume increases with increasing strain until approximately 20% strain with very little change in free volume at higher strains. Additionally, there is an interaction between the chain lengths and number of chains. For the shorter chain length of 100 monomer units, an increase in the number of chains translated to higher free volume values, whereas for longer chain lengths of 1000 monomer units, an increase in the number of chains had a negligible effect on free volume. The amorphous cells with longer chain lengths had higher free volume values than shorter chain lengths. Fig. 13 shows the effect of temperature on the change in free volume at a strain

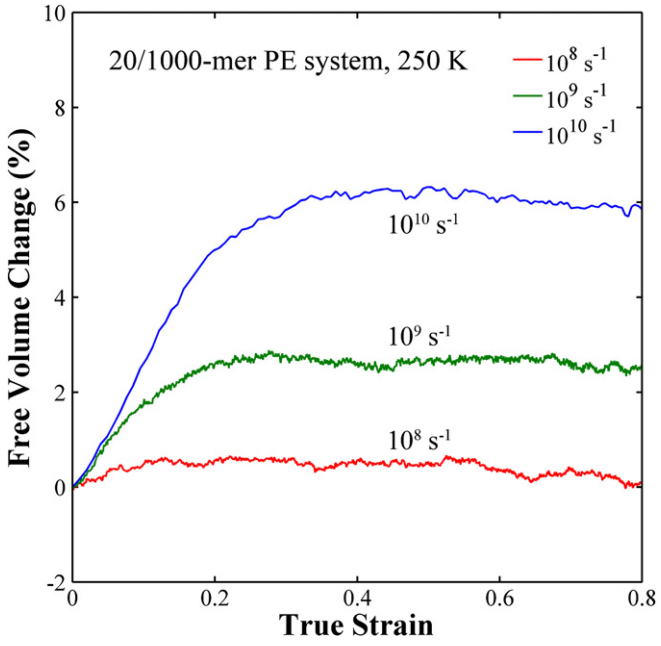

Fig. 11. Free volume evolution as a function of strain and strain rate (10^8 s^{-1}, 10^9 s^{-1}, and 10^{10} s^{-1}) for a polyethylene system with 20 chains consisting of 1000 monomers each at 250 K.

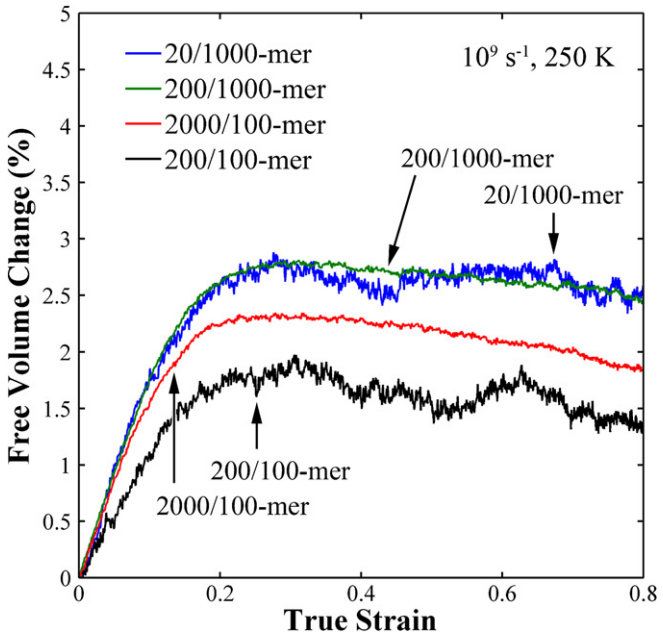

Fig. 12. Free volume evolution as a function of strain, chain length and number of chains at 250 K for a strain rate of 10^9 s^{-1}.

rate of 10^9 s^{-1} for temperatures of 100, 250 and 400 K. At 400 K, the free volume did not change appreciably. At 100 K and 250 K, the free volume increases with increasing strain until 20% strain followed by almost no change in the free volume.

The evolution of free volume change in the elastic regime of the stress-strain curves is also related to Poisson's ratio. Interestingly, the volumetric change for low strains indicates that Poisson's ratio is not constant in some cases, but is in fact evolving over the elastic regime. Calculations of the change in Poisson's ratio as a function of strain show that it monotonically decreases over this regime.

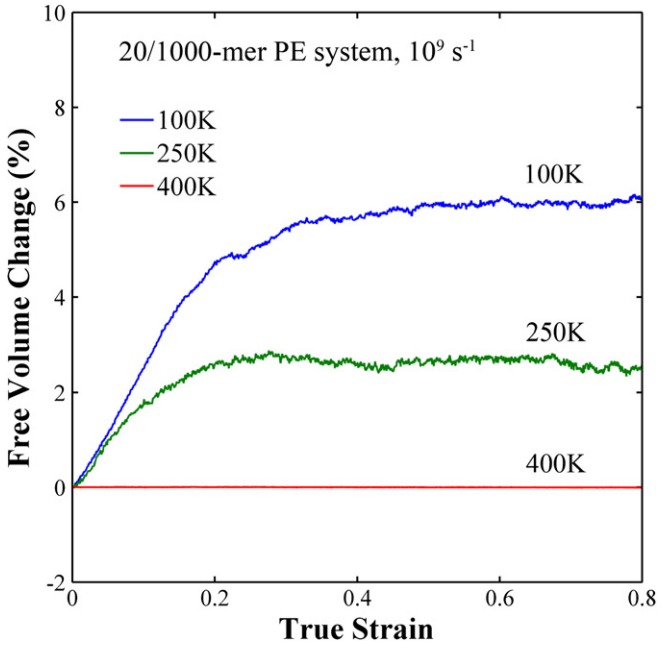

Fig. 13. Free volume evolution as a function of strain and temperature (100, 250, and 400 K) for a polyethylene system with 20 chains consisting of 1000 monomers each at a strain rate of 10^9 s^{-1}.

3.3.2. Chain bond length and angle evolution

The evolution of the bond length and bond angles as a function of strain can provide insight into the accommodation of deformation in glassy polymer structures. Fig. 14 shows how the (a) bond length and (b) bond angle distributions evolve as a function of strain at 250 K. The black line represents the mean values of the distributions while the upper (red) and lower (blue) markers represent the maximum and minimum values of the distributions, respectively. Additionally, this data is plotted for three different strain rates and for two different chain lengths/chain number combinations (20 1000-mer chains, 2000 100-mer chains) to ensure that this result is consistent across the different conditions examined herein. The minimum and maximum distribution values are plotted to give a sense of the evolution of the extreme values of the distributions. For instance, the maximum bond length would be important for deformation processes such as bond breaking along the polymer backbone. However, none of the metrics associated with the bond length or bond angle distributions show a significant change over the course of uniaxial deformation. This is, perhaps, as expected since the energy contributions from these components also did not show appreciable change as a function of strain. The present simulations clearly show that bond length and bond angle distributions change very little during deformation. The use of an

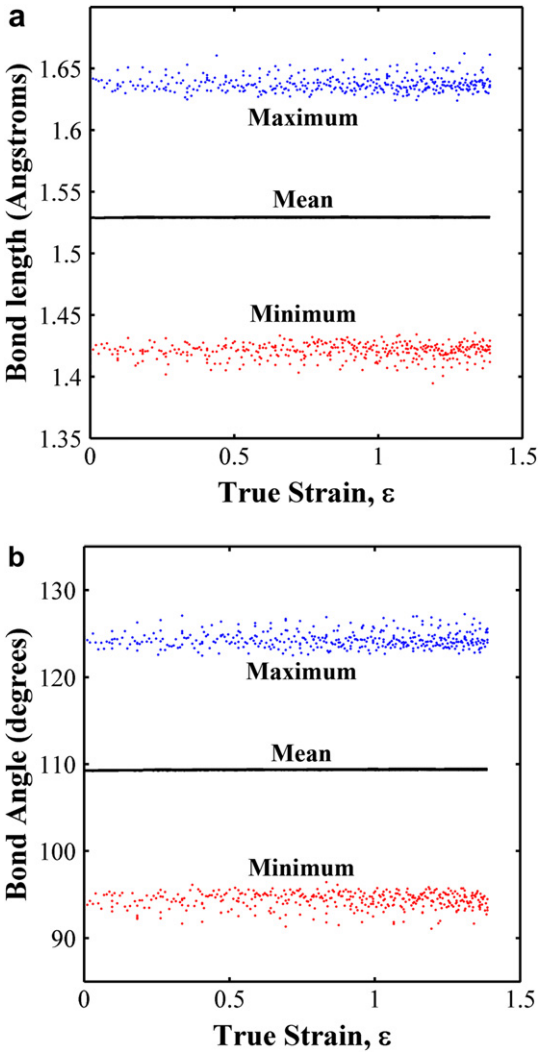

Fig. 14. (a) Bond length and (b) bond angle distributions as function of strain at 250 K.

interatomic potential that does not allow dynamic bond formation or scission seems to be valid since the bond length distribution is not changing. However, it is unclear as to whether fixed bond lengths and valence angles can be safely ignored during deformation simulations. For instance, the fact that the distribution does not seem to be changing does not mean that individual bond lengths and bond angles are not dynamically changing to allow dihedral rotations from *gauche* to *trans* conformations to reduce the energy of the system. Further studies could shed light on this area.

3.3.3. Chain dihedral conformation evolution

The change in the dihedral distribution from *gauche* to *trans* conformations as a function of strain is also important to deformation in polymer systems. Fig. 15 shows how the percent *trans* conformations evolves as a function of strain at 250 K. The percentage of *trans* conformations in the simulation cell was calculated using a threshold of 120° (see Fig. 15). Additionally, this data is plotted for three different strain rates and for two different chain lengths/chain number combinations (20 1000-mer chains, 2000 100-mer chains) to compare behavior between different conditions. First, the percent *trans* conformations increases at a faster rate as the strain rate decreases, i.e., a strain rate of $10^8\ s^{-1}$ has the fastest increase in trans conformations. This is as expected; the lower strain rate will allow more time for chains to rotate to trans conformations. However, the main difference between the three strain rates occurs in the elastic and strain softening regimes ($\varepsilon_{true} < 0.5$), and the increase in percent *trans* conformations during the strain hardening region is nearly constant. Notice that the $10^{10}\ s^{-1}$ strain rate shows very little increase in the percent *trans* conformations for the elastic region, in agreement with both previous simulations Capaldi et al. [30] and experimental NMR data [53]. The effect of the polymer chain length was also examined and one representative curve is included in Fig. 15 for comparison. For a strain rate of 10^9, the 2000 100-mer chain PE system shows very similar behavior to the 20 1000-mer chain system, when excluding the initially higher percent *trans* conformations in the former system.

3.3.4. Chain orientation evolution

The chain orientation as a function of strain is also an important microstructure response of the polymer chain segments during deformation. The chain orientation parameter used here combines two different methods presented within the literature. First, the local chain orientation at each atom i was computed from the vector connecting nearest neighbor atoms [25]: $e_i = (r_{i+1} - r_{i-1})/|r_{i+1} - r_{i-1}|$. Then, alignment of the chain segments corresponding to each atom in the direction of applied stress was calculated using

$$P_{2x} = \frac{3}{2}\left(\cos^2\left(\frac{e_i \cdot e_x}{|e_i||e_x|}\right)\right) - \frac{1}{2} \tag{4}$$

where e_x is the vector in the direction of applied stress (or orthogonal to the applied stress direction). In this manner, a value of 1 signifies pure chain segment alignment with the corresponding direction and a value of −0.5 signifies that the chain segment is orthogonal to the corresponding direction.

Fig. 16(a) shows an example histogram of the distribution of the chain orientation parameter for all chain segments with respect to the loading axis direction. Fig. 16(b) shows how the average chain

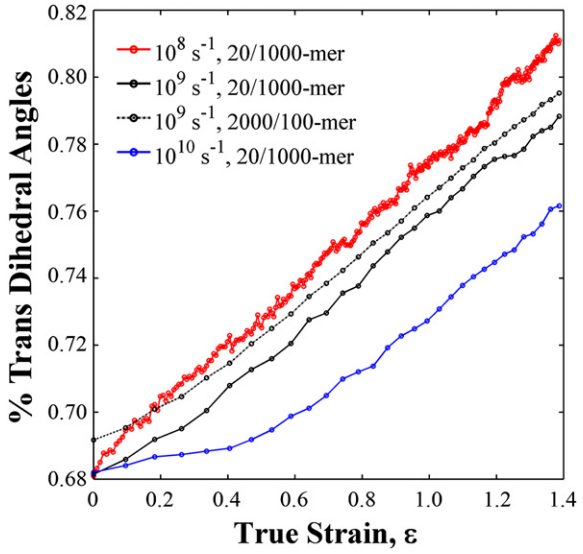

Fig. 15. Chain dihedral angle evolution as a function of strain for different strain rates, chain lengths, and number of chains at 250 K.

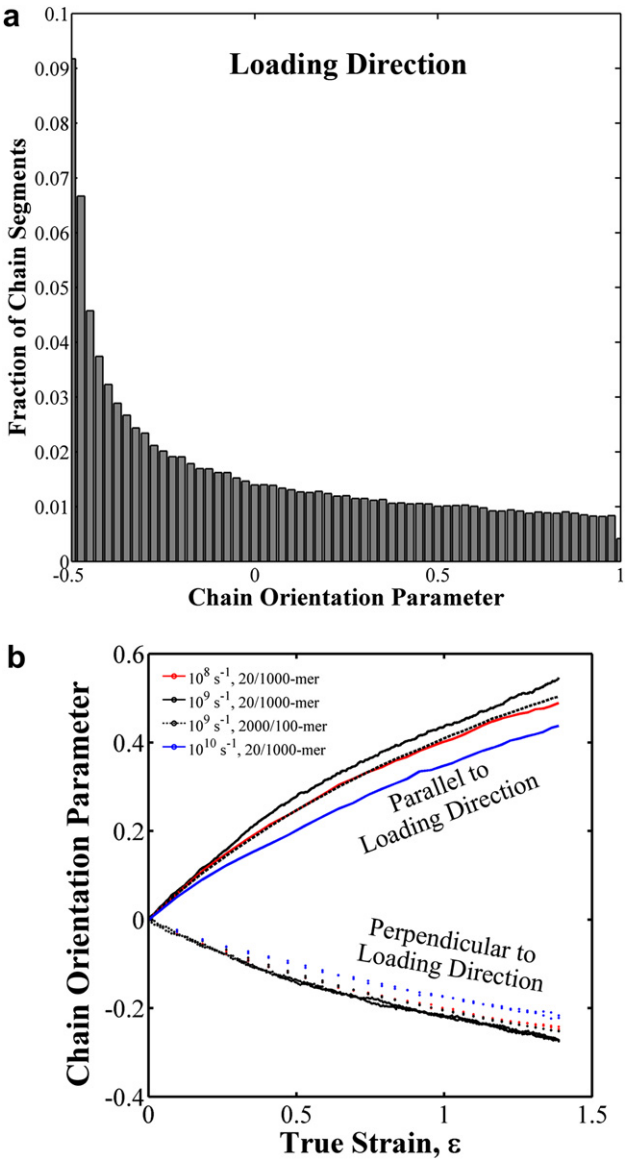

Fig. 16. Chain orientation evolution as a function of strain for different chain lengths and strain rates at 250 K. (a) The distribution of the chain orientation parameter in the loading direction, and (b) the mean chain orientation parameter as a function of strain.

orientation parameter, P_{2x}, evolves as a function of strain at 250 K. As with prior subsections, the four curves contain three different strain rates for the 20 1000-mer chain systems and an additional curve for a 2000 100-mer chain system at a strain rate of 10^9 s^{-1}. Not surprisingly, on average, the chain segments tend to align with the loading direction with increasing strain. Additionally, the strain rate has an effect on the observed alignment that increases at higher strains. However, the strain rate does not directly correlate with the magnitude of the chain alignment parameter, i.e., the values for the lowest strain rate falls between the two higher strain rates. Other factors or measured microstructure response variables may also contribute to chain orientation. Last, the shorter chain length (100-mer) system had a slightly lower alignment response than the larger chain length (1000-mer) system at the same strain rate.

3.3.5. Chain entanglement evolution

The chain entanglement evolution is also important for deformation of polymer systems. In general, fracture of many polymer materials is expected to occur due to chain disentanglement rather than chain scission, because of the strong carbon–carbon bonds in the polymer backbone. Here, we have used the geometric technique of Yashiro et al. [49] to calculate the chain entanglement. This technique first creates two vectors which emanate from each atom to neighboring atoms that are separated by 10 atoms on the same chain, i.e., one vector that connects atom i with atom $(i - 10)$ and one vector that connects atom i to atom $(i + 10)$. The angle between these two vectors is calculated for each applicable atom and a threshold parameter of 90° is used to specify if the atom is classified as entangled or not. The atoms classified as entangled via this technique are considered to be constrained by neighboring chains.

Fig. 17(a) shows an example histogram of the distribution of the angles calculated based on the Yashiro et al. [49] technique with a separation distance of 10 atoms. The number of atoms classified as entangled is then divided by the total number of applicable atoms to give a normalized entanglement parameter that can be used to compare the different systems. This entanglement parameter actually represents the percent of entangled atoms within the system and can be appropriately scaled by a constant to obtain the entanglement density. We refrain from using an entanglement density here, since this measure is dependent on the separation distance used for creating the two vectors and also the threshold parameter. However, these parameters simply affect the scaling of the *y*-axis and not the general trend. Fig. 17(b) shows the evolution of the entanglement parameter as a function of strain for three different strain rates and two chain lengths at 250 K. Notice that for the initial stages of deformation, the entanglement parameter remains somewhat constant with only a slight decrease. At higher strains, indicative of the strain hardening region, the entanglement parameter decreases in a linear fashion. As the strain rate is decreased, the entanglement parameter decreases at a faster rate in the strain hardening region. This is as expected; the lower strain rate will allow more time for chains to disentangle as a way to accommodate the deformation. A similar trend is observed for the shorter chain length system as well, although the entanglement parameter starts at a lower value. This is as expected as well; as the chain length decreases, the tendency should be for the chains to become more difficult to entangle. These results are in agreement with previous work of Tomita [50] and Shepherd [51], which assumes that the entanglement density decreases with an increase of the strain level at constant strain rate and temperature.

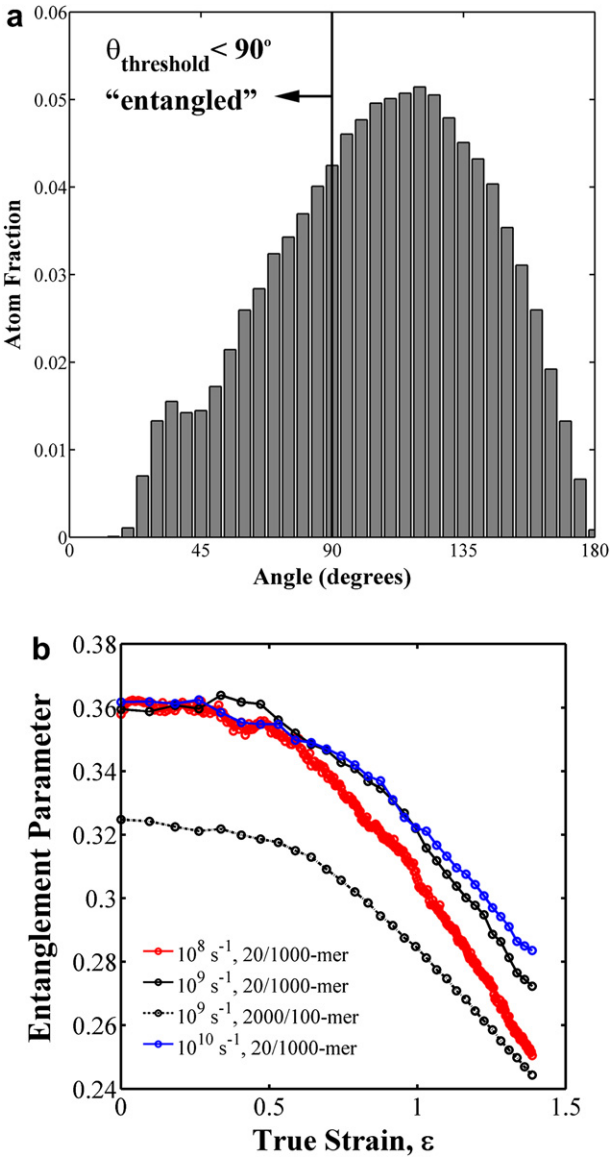

Fig. 17. Entanglement parameter evolution as a function of strain for different chain lengths and strain rates at 250 K. (a) The distribution of angles for the flexion node method and (b) the resulting entanglement parameter as a function of strain.

4. Discussion

MD simulations were performed to investigate the deformation mechanisms during uniaxial deformation of an amorphous PE-like polymer glass using a united atom model. The MD technique used here captures the structural behavior of an amorphous PE polymer as well as the deformation behavior over a wide range of loading conditions. The stress-strain behavior due to deformation shows a typical transition from the linear and nonlinear elastic regions at low strains, to yield, then to stress softening, and finally to strain hardening. We also qualitatively reproduced the dependence of the PE stress-strain behavior on strain rate, polymer chain length, and temperature. Although several groups [28,29,32,47,52] have tried to elucidate the thermomechanical behavior of amorphous PE polymers during deformation, the exact mechanism of the amorphous PE deformation is still a point of debate. In the present study, we attempt to shed light on the mechanisms of deformation in glassy polymers by examining the evolution of internal energy and chain conformations during mechanical deformation. This indicates that the deformation process can be divided into dominant mechanisms at several consecutive stages.

First, in the elastic region, the non-bonded interactions are dominant at higher strain rates as displayed by the increase in the

non-bonded energy. Since the non-bonded energy is described by the Lennard-Jones formulation for the van der Waal's forces, this indicates that deformation results in a deviation in the spacing between united atoms on adjoining chains. In the absence of torsional rotations (dihedral angle), as the polymer chains accommodate the elastic deformation, there is a net increase in the free volume which increases with increasing strain rate. At the lowest strain rate, torsional rotations were dominant in the elastic regime, which resulted in the highest rate of gauche-trans transformations, no increase in free volume, and very little increase in the non-bonded energy. However, qualitatively, the stress-strain behavior at the lowest strain rate deviates most from that observed in experiments, i.e., the characteristic yield peak is not as prominent as that at higher strain rates. Interestingly, these observations suggest that the characteristic yield peak is due, in part, to the dominant role of non-bonded interactions between chains combined with a lack of torsional rotation. Further, these mechanisms also explain the results of a more pronounced yield peak with decreasing temperature. Lower temperatures have fewer thermally-supported rotations, which resulted in increased non-bonded interactions and a higher yield peak. In addition, a comparison of the simulations with varying chain lengths solidifies the importance of non-bonded and rotational energies. Shorter chain lengths resulted in a lower entanglement parameter. With a lower entanglement parameter chains could more easily rotate and align with the direction of loading and thus had less pronounced yield peak. Noticeably absent in almost all conditions investigated is the role of bond length and bond angle during elastic deformation, which do not play a vital role.

As deformation progresses, the amount of mechanical work converted into the non-bonded energy decreases. The non-bonded interaction energy decreases as the chains accommodate deformation through torsional processes, which straighten, unfold, and align the chains in the direction of loading. These intra-chain processes result in the transformation of gauche to *trans* conformations (Fig. 15) and a corresponding decrease in the torsional (dihedral) energy. The free volume evolution is fairly constant in this regime, indicating that changes in the chain conformations and alignment do not significantly impact the spacing between chains. Instead, the results here suggest that for certain strain rates and temperatures, a minimum amount of free volume is a requirement for further deformation within the chains via torsion. The present study shows that this deformation mechanism depends more strongly on external conditions, like temperature and strain rate, than the length of the chains or the number of chains.

The boundary conditions used in atomistic simulations of deformation in material systems needs to be further investigated for polymeric systems. For instance, in the present simulations, the total energy decreases at large strains. However, the uniaxial stress increases over the same strains, implying that additional work is being done to the system (which should result in an increase in internal energy). These responses seem to be contradictory. However, since the thermostat for the NPT boundary conditions is maintaining the temperature of the system through adjusting the atom velocities, the additional work generated in the strain hardening region is being dissipated at a rapid rate through the Nose-Hoover thermostat. Currently, it is not known how removing the thermostat or adjusting the rate of heat dissipation in atomistic simulations will impact the energy distribution at higher strains. Future work will explore how the rate of heat dissipation impacts these considerations at the molecular scale.

5. Conclusions

Molecular dynamics (MD) simulations were used to study the main deformation mechanisms responsible during uniaxial tensile loading of an amorphous polyethylene (PE)-like polymer. These simulations were performed for different strain rates and temperatures under uniaxial tensile loading to investigate the influence of these external factors on mechanical properties of PE polymer. Results show that many mechanical properties of PE can be simulated by MD in qualitative some times in quantitative agreement with experiments.

i) The simulated stress-strain behavior at the strain rate of 10^{10} s^{-1} (Fig. 3) shows the same trends as those observed in experimental testing for amorphous polymers, i.e., an elastic regime followed by a yield peak and subsequent softening and strain hardening regimes. The characteristic yield peak observed in polymers decreases with increasing temperature (Fig. 5) and decreasing strain rate (Fig. 6). This difference provided the contrast between conditions that was necessary for exploring what mechanisms were responsible for the characteristic yield peak in polymers. Over all the strain rate and temperature have much stronger effect on the behavior than chain length and number of chains, which show little effect on the stress-strain behavior (Fig. 4).
ii) In the elastic and yield peak regimes, the energy evolution plots show that interchain non-bonded (Van der Waal's) interactions played a significant role, as shown by the amount of the total potential energy increase that is due to the non-bonded energy (Figs. 7–10). This increase in energy is later associated with an increase in the free volume (Fig. 11), which is required prior to intra-chain torsional processes for some conditions. The evolution of free volume also suggests that Poisson's ratio evolves within the elastic regime.
iii) In the strain softening and hardening regimes, the energy evolution plots show that intra-chain torsion mechanisms played a significant role (Figs. 7–10). This decrease in dihedral energy is later associated with the transformation of gauche conformations to lower energy *trans* conformations (Fig. 15). Additionally, an entanglement parameter calculated from the intra-chain geometry shows that the majority of disentanglement occurs in this regime (Fig. 17).
iv) The present simulations clearly show that the bond length and bond angle distributions remain nearly constant over all regimes for all conditions (Fig. 14). This is also supported by the minimal change in energy associated with bond length and bond angle compared to the non-bonding and dihedral energy changes.
v) Chain alignment in the direction of loading increases with increasing strain over all regimes (Fig. 16).

Future investigation will focus in building a hierarchical multiscale approach using the information obtained from the molecular dynamic scale (e.g. evolution of free volume and entanglement density with deformation, strain rate, temperature) to refine the continuum level constitutive model (see Bouvard et al. [54] for more details).

Acknowledgement

The authors would like acknowledge financial support through the Center for Advanced Vehicular Systems at Mississippi State University. Additionally, the authors would like to acknowledge the insightful comments from the reviewers during the review process.

References

[1] Van Krevelen DW. Properties of polymers. 3rd ed. , Amsterdam: Elsevier; 1990.
[2] Bouvard JL, Ward D, Hossain D, Marin EB, Horstemeyer MF. JEMT, Special Issue: Predictive Science & Technology in Mechanics & Materials, 2009;131: 041206.

[3] Baschnagel J, Binder K, Doruker P, Gusev AA, Hahn O, Kremer K, et al. Bridging the gap between atomistic and coarse-grained models of polymers: status and perspectives. In: Advances in polymer science: viscoelasticity, atomistic models, Statistical Chemistry; 2000. p. 41–156.
[4] Paul W, Yoon DY, Smith GD. J Chem Phys 1995;103(4):1702–9.
[5] Yoon DY, Smith GD, Matsuda T. J Chem Phys 1993;98(12):10037–43.
[6] Faller R, Muller-Plathe F. Polymer 2002;43(2):621–8.
[7] Fukunaga H, Takimoto J, Doi M. J Chem Phys 2002;116(18):8183–90.
[8] Kremer K. MRS Bulletin 2001;26(3):205.
[9] Müller-Plathe F. ChemPhysChem 2002;3(9):754–69.
[10] Uhlherr A, Theodorou DN. Curr Opin Solid State Mater Sci 1998;3(6):544–51.
[11] Eyring H. J Chem Phys 1936;4:283.
[12] Robertson R. J Chem Phys 1966;44:3950.
[13] Argon AS. Philos Mag 1973;28:839.
[14] Deng D, Argon AS, Yip S. Philos Trans R Soc London 1989;A329:613.
[15] Maeda K, Takeuchi S. Philos Mag 1981;A44:643.
[16] Srolovitz D, Vitek V, Egami T. Acta Metall Mater 1983;31:335.
[17] Theodorou D, Suter U. Macromolecules 1985;18:1467.
[18] Theodorou D, Suter U. Macromolecules 1986;19:139.
[19] Mott P, Argon AS, Suter U. Philos Mag 1993;67:931.
[20] Hutnik M, Argon AS, Suter U. Macromolecules 1993;26:1097.
[21] Brown D, Clarke J. Macromolecules 1991;24:2075.
[22] McKechnie J, Clarke J. Macromolecules 1993;26:198.
[23] Depa PK, Maranas JK. J Chem Phys 2005;123(9):094901.
[24] Depa PK, Maranas JK. J Chem Phys 2007;126(5):054903.
[25] Lavine MS, Waheed N, Rutledge GC. Polymer 2003;44:1771–9.
[26] Pearson DS, Ver Strate G, Von Meerwall E, Schilling FC. Macromolecules 1987;20(5):1133–41.
[27] Tries V, Paul W, Baschnagel J, Binder K. J Chem Phys 1997;106(2):738–48.
[28] Capaldi FM, Boyce MC, Rutledge GC. Phys Rev Lett 2001;89. 175505-1–4.
[29] Capaldi FM, Boyce MC, Rutledge GC. Polymer 2004;45:1391–9.
[30] Yang L, Srolovitz DJ, Yee AF. J Chem Phys 1999;110(14):7058–69.
[31] Takeuchi H, Roe RJ. J Chem Phys 1991;94:7458–65.
[32] Li J, Mulder T, Vorselaars B, Lyulin AlexeyV, Michels MAJ. Macromolecules 2006;39(22):7774–82.
[33] Ospina SA, Hess M, Lopez BL. e-Polym 2004;024.
[34] Ospina SA, Restrepo J, Lopez BL. Mater Res Innov 2003;7:27–30.
[35] Brostow W, Corneliussen RD. Failure of Plastics. Newyork: Hanser; 1986.
[36] Mayo SL, Olafson BD, Goddard III WA. J Phys Chem 1990;94:8897.
[37] Shepherd JE, McDowell DL, Jacob KI. J Mech Phys Solids 2006;54:467.
[38] Shepherd JE. Multiscale modeling of the deformation of semi-crystalline polymers, Ph.D. thesis, Georgia Institute of Technology, Atlanta, GA 2006.
[39] Plimpton SJ. Computational Phys 1995;117(1):1–19.
[40] Nosé SJ. Chem Phys 1984;81:511–9.
[41] Hoover WG. Phys Rev A 1985;31:1695–7.
[42] Lyubartsev A. Eur Biophys J 2005;35(1):53–61.
[43] Binder K. Monte Carlo and molecular dynamics simulations in polymer science. New York: Oxford University Press; 1995.
[44] Han J, Gee RH, Boyd RH. Macromolecules 1994;27(26):7781–4.
[45] Rigby D, Roe RJ. J Chem Phys 1987;87(12):7285–92.
[46] Gee RH, Boyd RH. J Comput Theor Polym Sci 1998;8:93–8.
[47] Brandrup J, Immergut EH. Polymer handbook. 3rd ed. New York: Wiley-Interscience; 1989.
[48] Melchionna S, Ciccotti G, Holian BL. Mol Phys 1993;78(3):533–44.
[49] Yashiro K, Ito T, Tomita Y. Int J Mech Sci 2003;45:1863–76.
[50] Tomita Y. Int J Mech Sci 2000;42:1455–69.
[51] Shepherd JE, McDowell D, Jacob KI. J Mech Phy Solids 2006;54:467–89.
[52] Chui C, Boyce MC. Macromolecules 1999;32(11):3795–808.
[53] Utz M, Atallah AS, Robyr P, Widmann AH, Ernst RR, Suter UW. Macromolecules 1999;32:6191–205.
[54] Bouvard JL, Ward DK, Hossain D, Marin EB, Bammann DJ, Horstemeyer MF. Acta Mechanica 2010;213:71–96.